

Article

Enhanced Electrodesorption Performance via Cathode Potential Extension during Capacitive Deionization

Jie Fu ¹, Haifang Wang ¹, Riya Jin ¹, Pengxiao Liu ¹, Ying Li ¹, Yunyan Wang ^{2,3}, Qingwei Wang ^{2,3,*} and Zhumei Sun ^{1,2,*}

¹ School of Environmental and Safety Engineering, North University of China, Taiyuan 030051, China; fujietg@163.com (J.F.); whfang@nuc.edu.cn (H.W.); jrya@nuc.edu.cn (R.J.); lpx@nuc.edu.cn (P.L.); lum0610@gmail.com (Y.L.)

² School of Metallurgy and Environment, Central South University, Changsha 410083, China; wyy@csu.edu.cn

³ Chinese National Engineering Research Center for Control & Treatment of Heavy Metal Pollution, Changsha 410083, China

* Correspondence: qw_wang@csu.edu.cn (Q.W.); sunzhumei41@163.com (Z.S.)

Abstract: Complete desorption of contaminants from electrode materials is required for the efficient utilization and long service life of capacitive deionization (CDI) but remains a major challenge. The electrodesorption capacity of CDI in the conventional electrode configuration is limited by the narrow electrochemical stability window of water, which lowers the operating potential to approximately 1.2 V. Here, we report a graphite anode–titanium cathode electrode configuration that extends the cathode potential to -1.7 V and provides an excellent (100%) electrodesorption performance, which is maintained after five cycles. The improvement of the cathode potential depends on the redox property of the electrode. The stronger the oxidizability of the anode and reducibility of the cathode, the wider the cathode potential. The complete desorption potential of SO_4^{2-} predicted by theoretical electrochemistry was the foundation for optimizing the electrode configuration. The desorption efficiency of Cl^- depended on the ionic strength and was negligibly affected by circulating velocities above 112 mL min^{-1} . This work can direct the design optimizations of CDI devices, especially for reactors undergoing chemisorption during the electrosorption process.

Keywords: capacitive deionization; electrodesorption; cathodic polarization; cathode potential; chloride ion



Citation: Fu, J.; Wang, H.; Jin, R.; Liu, P.; Li, Y.; Wang, Y.; Wang, Q.; Sun, Z. Enhanced Electrodesorption Performance via Cathode Potential Extension during Capacitive Deionization. *Appl. Sci.* **2022**, *12*, 2874. <https://doi.org/10.3390/app12062874>

Academic Editor: Dong Kook Kim

Received: 14 January 2022

Accepted: 8 March 2022

Published: 10 March 2022

Publisher's Note: MDPI stays neutral with regard to jurisdictional claims in published maps and institutional affiliations.



Copyright: © 2022 by the authors. Licensee MDPI, Basel, Switzerland. This article is an open access article distributed under the terms and conditions of the Creative Commons Attribution (CC BY) license (<https://creativecommons.org/licenses/by/4.0/>).

1. Introduction

Capacitive deionization (CDI), often referred to as electrosorption, is the process of driving counter ions toward an electrode by applying an electrical potential between two electrodes [1–4]. Ions such as Cl^- , F^- , HCO_3^- , SO_4^{2-} , NO_3^- , ClO_4^- , K^+ , Na^+ , Mg^{2+} , Ca^{2+} , Cd^{2+} , Pb^{2+} , and Cu^{2+} are held at the electrode–solution interface by an electrical double layer (EDL) formed under the applied potential [5,6]. CDI is easily operated under ambient conditions and low voltages (1.2 V) without requiring high-pressure pumps, thermal heaters, distillation columns, or membranes [7,8]. Therefore, electrosorption has attracted widespread attention in the adsorption processes of brackish water desalination [9–12], wastewater treatment [13,14], and the purification of supplied water [6,15,16].

More importantly, in CDI based on EDL theory, contaminants from the electrodes can be easily removed by shorting or reversing the electrodes in the absence of chemicals [17]. However, this scenario is true only in ideal CDI operations, when the amount of charge during adsorption equals that during desorption. In fact, electrodesorption by shorting or reversing the electrodes cannot completely desorb the contaminants. Lee et al. [18] reported a 40–46% desorption efficiency at 10 mA/cm^2 . Lado et al. [19] studied different regeneration modes—open-circuit potential (OCP), short circuit (SC), and reverse voltage (RV)—in a CDI system equipped with asymmetric electrodes. The highest regeneration

recovery in their study was 64%. Many recent research studies have reached similar conclusions [20–22]. Electrodesorption is a widely acknowledged problem in CDI and has defied solutions because the key factors of the existing regeneration technology remain unclear. The incomplete regeneration of electrode materials has increased the cost of electroadsorption and inevitably introduced secondary pollution.

This study employs a three-dimensional electrode reactor with the characteristics of many small particles, which shortens the transfer distance between the reactant and the electrode and hence increases the specific surface area of the working electrode [23–26]. However, recycling smaller particles from a solution in a three-dimensional electrode reactor is a difficult task and risks forming a new environmental pollutant [24]. Porous carbons such as activated carbon [25,27], activated carbon fibers [28], and carbon aerogels [29] are commonly used as electroadsorption electrode materials. Activated carbon is a popular choice, especially for particle electrodes in three-dimensional electrode reactors, owing to its high electrical conductivity, good mechanical strength, and low cost [30–33]. Under an electric field, the particles in a particle electrode can carry the same charge as the adjacent electrode. Hence, electrode matching is another key requirement of three-dimensional electrode reactors. If the electrodes are well matched, the overall performance of the electrodesorption process is improved. Poorly matched electrodes can degrade the performance or cause electrode damage [34,35].

The present study on the electrodesorption process is based on our previous three-dimensional electrode system but focuses on electrode matching to improve the cathode potential. According to theoretical electrochemistry, the cathode potential plays a definitive role. Here, the complete desorption potential is predicted in a theoretical electrochemistry analysis, and the extended cathode potential after matching the electrodes is discussed in detail. After performing electroadsorption and desorption cycles, the electrode configuration and the predicted complete desorption potential are applied to the electrodesorption of SO_4^{2-} . The effects of ionic strengths and circulation velocities on the desorption efficiency are evaluated in electrodesorption batch tests.

2. Experimental

2.1. Apparatus

The three-dimensional electrode system adopted in the electrodesorption investigation was similar to our previous studies [36–38], and a structure diagram of the system is shown in Figure 1.

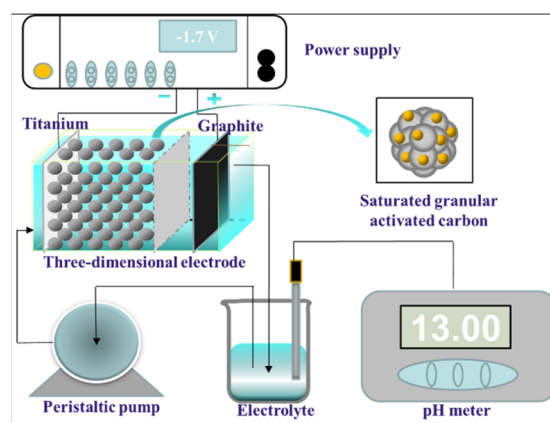


Figure 1. The reaction equipment in electrochemical experiments.

2.2. Materials and Methods

All chemical reagents used for the experiments were analytically pure. All granular activated carbon (GAC) was purchased from Youshi Technology Co., Ltd. (Ningbo, China), and the characterization of the GAC was analyzed in our previous work [36].

The electrosorption of Cl^- on GAC given here is based on our previous studies [37,38]. The desorption of Cl^- was studied via two steps of experiments using a three-dimensional electrode reactor at room temperature. First, after the completion of electrosorption, the electrical field was removed, and the desorption solution was circulated at a flow rate of 112 mL min^{-1} . After 3 h, desorption without cathodic polarization was complete, and a -1.7 V cathode potential was immediately applied to the device. The pH of the desorption solution was measured throughout the experiment to ensure that the pH was maintained at the initial pH. Samples were taken from the reactor at different sampling times (15, 30, 60, 120, 180, 240, and 300 min).

The anion concentration was detected by ion chromatography (IC) (833 Basic IC Plus, Metrohm Ltd., Herisau, Switzerland) with an anion separation column (Metrosep A Supp 4) and an IC conductivity detector. The desorption efficiency (De) of GAC was calculated according to the following equation:

$$De = \frac{m_w}{m_e} \times 100 \quad (1)$$

where m_e (mg) and m_w (mg) are the mass of the anions adsorbed on the GAC and then desorbed in the regenerated solution, respectively.

The anode and cathode potentials were measured in the three-electrode system. A saturated calomel electrode (SCE) is used as the reference electrode and submerged in the electrolytes. In this paper, all potentials are given relative to this electrode. A hole with a diameter of 4 mm was opened at the lower half of electrodes for the salt bridge to cross and fix. The potentials were monitored by a digital multimeter (UNI-T UT139C Bench Digital Multimeter, Shanghai, China).

3. Results and Discussion

3.1. Electrosorption and Desorption Cycles

Adsorption experiments were performed at 1.2 V and with open-circuit potential (OCP). The experimental operations are detailed in our previous studies [38]. Figure 2a plots the adsorption capacity of chloride ions over time. The Cl^- adsorption capacity on GAC increased from $12.76 \mu\text{mol g}^{-1}$ to $18.11 \mu\text{mol g}^{-1}$ as the anode potential rose from the OCP to 1.2 V , reflecting the formation of an electric double layer between the electrode surface and chloride ions. Similar phenomena have been reported by other studies [18,39]. Figure 2b plots the desorption efficiency over time in the absence and presence of cathodic polarization. The experimental results indicate that Cl^- was desorbed with an efficiency of 83% when the electric field vanished for 1 h. Unfortunately, 17% of the residual Cl^- failed to desorb from the GAC surface, even after extending the desorption time, implying that 100% desorption is almost impossible by chemical regeneration. This result is consistent with Zhang et al. [40], who studied the adsorption of F^- on a novel zirconium-modified-Na-attapulgite (Zr-A) adsorbent. They also reported that desorption could not reach 100% within 120 min at pH 12.50, especially after six desorption-adsorption cycles. This might be attributed to chemical adsorption occurring in the electrosorption process. Lai et al. [41] similarly found that after the adsorption of phosphate, the regeneration rate of the absorbent material failed to reach 100% under a reversed potential for 10 min, because chemisorption is the main adsorption mechanism. Previously [36], we reported that the Cl^- adsorption mechanism at a GAC surface is hydrogen bonding. This mechanism was confirmed by monitoring the changes in anode potential on the GAC at different times. In these experiments, the Cl^- electrolyte was continuously recycled at cell voltages of 0.3 and 1.0 V. The anode potentials on GAC at different times are shown in Figure 2d. As the time increased from 15 to 300 min at a cell voltage of 1.0 V, the anode potential increased from 1.01 to 1.35 V. A similar phenomenon was observed when the cell voltage is 0.3 V. This behavior can be explained as follows: When an anion is chemisorbed, the anions near the surface tend to drive the electrons back into the electrode and the anode potential increases [42]. Therefore, chemical bonds are inferred to be involved in the electrosorption

process, consolidating the results of our previous theoretical analysis [43]. Biesheuvel et al. also reported that ions can be physically and chemically adsorbed in the diffusion layer of the double layer [44]. For this reason, after removing the electric field, the electroadsorbed Cl^- in the EDL was released into the solution but the chemically adsorbed Cl^- was not desorbed; consequently, 17% of the Cl^- remained. Xing similarly found that humics adsorbed by chemical adsorption on carbon electrodes were often inefficiently desorbed in the regeneration process [45]. However, as shown in Figure 2c, residual Cl^- was completely desorbed under a -1.7 V cathode potential applied for 1 h, indicating that cathodic polarization can effectively desorb chemically adsorbed Cl^- . Thereafter, successive electroadsorption and regeneration were achieved by circulating the solution. The duration of each electroadsorption and regeneration phase was 5 h. Figure 2c plots the Cl^- concentration at the inlet and outlet over five consecutive electroadsorption/regeneration cycles. The Cl^- adsorption capacity was maintained with no sharp declines throughout the five cycles, and the electrodesorption performance was maintained at 100% during consecutive cycles. According to these results, cathodic polarization can effectively enhance the desorption ability for sustainable operation, thereby improving the practicability of CDI.

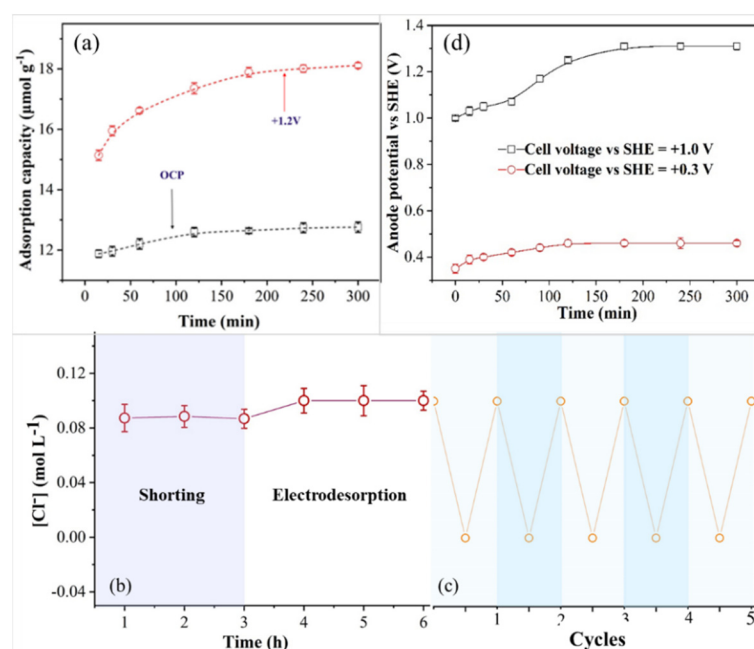


Figure 2. Electroadsorption and desorption cycles. (a) Comparison of Cl^- adsorption capacity at OCP and 1.2 V. (b) The concentration of Cl^- with and without cathodic polarization (c) cycles for adsorption and electrodesorption. (d) The curve of anode potential changed with cell voltage in the electroadsorption process.

3.2. Effect of Electrode Configuration

To study the key factors for Cl^- complete desorption more intensively, electrodesorption experiments were explored by varying the electrode configuration. The operation was carried out by assembling the electrodes in five configurations, as shown in Table 1, where two were symmetric and three were asymmetric. The cathode potential was measured by adjusting the cell voltage and controlling the anode potential to +1.2 V, which is the electrochemical stability window of water [46]. In addition, Cl^- oxidation may occur in the presence of the NaCl electrolyte [47–49] when the anode potential is higher than +1.2 V. However, when the anode potential was +1.2 V for Group 2, the cell voltage reached +15 V. To take into consideration the energy consumption, the measurement experiment of Group 2 was performed at the same cell voltage as that for Group 5. Figure 3a and Table 1 show the experimental data measured in the three-electrode system. Clearly, the cathode potential of Group 5 (-1.08 V) is higher than that of the other groups, which was determined under

the same anode potential (+1.2 V), especially for the titanium anode–titanium cathode combination. However, the cathode potential of Group 5 is much less than that of Group 2 (−1.7 V) when determined at the same cell voltage. These results indicate that the cathode potential is dependent on the electrode configuration, which decreased in the order of Group 2 > Group 5 > Group 3 > Group 4 > Group 1. Five sets of desorption experiments were performed under the acquired cathode potential. After 5 h, the desorption experiments were nearly complete, and the results are shown in Figure 3b. The desorption efficiency increased as the desorption time increased from 0 to 300 min for all groups. However, after 5 h, Group 2, Group 5, and Group 3 exhibited higher desorption efficiencies of 100%, 95%, and 68%, respectively, compared with Group 4 and Group 1, with values of 52% and less than 30%, respectively. The results indicate that different electrode combinations greatly influence the desorption efficiency because the cathode potential depends on the electrode combinations. Furthermore, an asymmetric electrode structure (G-Ti, G-Pb, and G-Cu) is more propitious to the electrodesorption of Cl^- than a symmetrical structure (Ti-Ti and G-G). In comparison to the previous reports, the desorption efficiency was higher in our work (Table 2). However, further optimization of the operating conditions will be needed for decreasing the desorption time.

Table 1. The different electrode configurations within the CDI devices for the experiments.

Group	Anode	Cathode	Sign	Cathode Potential/V
1	Titanium (Ti)	Titanium (Ti)	Ti-Ti	−0.22
2	Graphite (G)	Titanium (Ti)	G-Ti	−1.70
3	Graphite (G)	Lead (Pb)	G-Pb	−0.88
4	Graphite (G)	Graphite (G)	G-G	−0.71
5	Graphite (G)	Copper (Cu)	G-Cu	−1.08

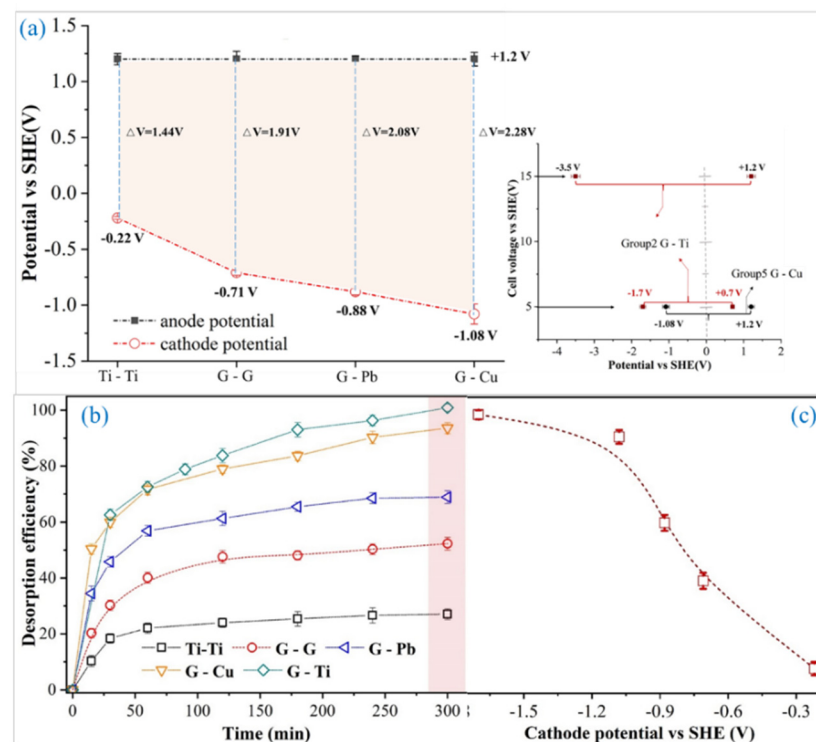


Figure 3. Effect of electrode configuration. (a) The cathode potential development of different electrode types. (b) The desorption efficiency of Cl^- using different electrode types. (c) The corresponding cathode potential (pink streak).

Table 2. The comparison of desorption efficiency.

Electrode	Reference	Desorption Efficiency/%	Time/min	Potential/V
GAC	This study	100	300	−1.7
Fe ₂ O ₃ /NORIT	[50]	64	480	−3.0
Fe ₂ O ₃ /G5	[50]	80	480	−3.0
LiMn ₂ O ₄	[51]	<45	500	3.5

It is worth noting that the broadest cathode potentials measured in Group 2 and Group 5 were −1.7 V and −1.08 V, respectively, at a cell voltage of +5.0 V (Figure 3a). The anode potentials were +0.7 V and +1.2 V, respectively, implying that as the anode potential of Group 2 increased continuously to +1.2 V, the scope of the cathode potential broadened (−3.5 V in Figure 3a). That is, the graphite anode–titanium cathode electrode configuration facilitated the extension of the cathode potential under the same conditions. This behavior may be attributed to the different reducibilities and oxidizabilities of the different electrode materials. In Groups 2, 3, 4, and 5, the reducibility values of the cathode materials increased in the order of G < Cu < Pb < Ti, and the desorption efficiencies at the cathode decreased in the order of Ti > Cu > Pb > G. Clearly, the reducibility declined, resulting in a desorption efficiency decrease, although deviations appeared at the Cu and Pb cathodes. This discrepancy might be related to the formation of an oxidation film on the surface of the lead electrode in air. Supporting this idea, the researcher None stated that lead is easily and rapidly oxidized to lead oxide over a wide temperature range [52]. Anode oxidizability also significantly affects the desorption efficiency. The higher oxidizability of the graphite anode than that of titanium likely explains the lower desorption efficiency of Group 1 than of Group 2. Therefore, the cathode potential might be extended by increasing the oxidizability and reducibility discrepancies between the anode and cathode. This conclusion provides a direction for optimizing the design of CDI devices, especially reactors that undergo chemisorption during the electrosorption process.

The electrodesorption process was also described based on theoretical electrochemistry. The desorption reaction for adsorbed Cl[−] from the GAC surface can be described by the following simple chemical equation



where ads and aq denote the adsorbed phase and solution phase, respectively.

The electrochemical potential of Cl[−] adsorbed on GAC and that in the solution can be expressed as:

$$\bar{\mu}_{\text{aq}} = \mu_{\text{aq}}^{\theta} + RT \ln [\text{Cl}^-_{\text{aq}}] - \psi_0 F \quad (3)$$

$$\bar{\mu}_{\text{ads}} = \mu_{\text{ads}}^{\theta} + RT \ln [\text{Cl}^-_{\text{ads}}] - \psi F \quad (4)$$

where μ_{aq}^{θ} and $\mu_{\text{ads}}^{\theta}$ are the standard state chemical potentials of Cl[−] in the liquid phase and in the solid phase, respectively, R (8.314 J mol^{−1} K^{−1}) is the universal gas constant, T (K) is the absolute temperature, F (96485 C mol^{−1}) is the Faraday constant, ψ_0 (V) is the potential of the solution, and ψ is the diffuse layer potential (where the value is relative to the potential of the solution (ψ_0)).

When the desorption of adsorbed Cl[−] occurs, the Gibbs free energy change ($\Delta_r G_m$) is given by:

$$\Delta_r G_m = \mu_{\text{aq}}^{\theta} + RT \ln [\text{Cl}^-_{\text{aq}}] - \psi_0 F - (\mu_{\text{ads}}^{\theta} + RT \ln [\text{Cl}^-_{\text{ads}}] - \psi F) \quad (5)$$

where μ_{aq}^{θ} and $\mu_{\text{ads}}^{\theta}$ are the standard-state chemical potentials of Cl[−] in the liquid phase and in the solid phase, respectively; ψ is the diffuse layer potential (where the value is

relative to the potential of the solution (ψ_0), and ψ_0 is the potential of the solution, whose value is zero; therefore, Equation (5) is expressed as:

$$\Delta_r G_m = \mu_{aq}^\theta - RT \ln [\text{Cl}_{aq}^-] - \mu_{ads}^\theta - RT \ln [\text{Cl}_{ads}^-] + \psi F \quad (6)$$

and, finally

$$\Delta_r G_m = \mu_{aq}^\theta - \mu_{ads}^\theta + RT \ln \frac{[\text{Cl}_{aq}^-]}{[\text{Cl}_{ads}^-]} + \psi F \quad (7)$$

In the desorption process, the standard Gibbs free energy change of uncharged particles transferred from a solid phase to a liquid phase is the same as the difference in the chemical potential between the solid phase and the liquid phase. Therefore, the standard Gibbs free energy change in the standard state can be expressed as:

$$\Delta_r G_m^\theta = \mu_{aq}^\theta - \mu_{ads}^\theta \quad (8)$$

The standard Gibbs free energy change is given by:

$$\Delta_r G_m^\theta = -RT \ln K_d \quad (9)$$

where K_d is the desorption equilibrium constant.

According to Equations (8) and (9), we obtain

$$\Delta_r G_m = -RT \ln K_d + RT \ln \frac{[\text{Cl}_{aq}^-]}{[\text{Cl}_{ads}^-]} + \psi F \quad (10)$$

If

$$Q = \frac{[\text{Cl}_{aq}^-]}{[\text{Cl}_{ads}^-]} \quad (11)$$

Inserting Equation (11) into Equation (10), we obtain

$$\Delta_r G_m = -RT \ln K_d + RT \ln Q + \psi F \quad (12)$$

and, then

$$\Delta_r G_m = RT \ln \frac{Q}{K_d} + \psi F \quad (13)$$

When desorption reaction reaches equilibrium, Equation (13) can be expressed as:

$$RT \ln \frac{Q}{K_d} = -\psi F \quad (14)$$

If cathodic polarization occurs, then the value of parameter ψ is negative.

$$-\psi F > 0 \quad (15)$$

Thus, Equations (13) and (15) show that Cl^- on the GAC surface is desorbed and entered the solution because the Gibbs free energy change exceeded 0 when the cathode was polarized. This is consistent with the experimental electrodesorption results at different cathode potentials (Section 3.2), implying that Cl^- desorption is affected by cathodic polarization in the CDI process. However, as confirmed in the experimental electrodesorption results, the desorption efficiency cannot reach 100% when the cathode potential cannot reach -1.7 V; that is, the cathode potential distribution must be sufficient to completely desorb Cl^- . The Gibbs free energy of desorption depends on the cathode potential;

specifically, as the range of cathode potential broadens, the desorption becomes easier. Based on the above analysis, we speculated that the incomplete desorption of the electrode in previous studies [18,19,41], even under cathodic polarization, is linked to insufficient cathode potential.

The electrodesorption process has successfully predicted the complete desorption potential (ψ) that achieves complete Cl^- desorption. The parameter $[\text{Cl}^-_{\text{aq}}]$ represents the Cl^- concentration in solution when the Cl^- have completely desorbed from the GAC electrode, which can be derived from the equilibrium absorption capacity. The other parameter $[\text{Cl}^-_{\text{ads}}]$ represents the amount of Cl^- adsorbed on the GAC surface. Its value is nearly zero when the Cl^- completely desorbs, but for a convenient calculation, we replaced the value of $[\text{Cl}^-_{\text{ads}}]$ by the detection limit of the ion chromatograph. During the electrodesorption process, K_d was calculated by the method reported in our previous research [38]. By Equations (11) and (13), the parameter ψ (i.e., the potential of complete desorption) was determined as -1.64 V, close to the experimental value. Based on the above research, anions' electrodesorption can be carried out by matching the electrode configuration after predicting the complete desorption potential.

3.3. Application to Electrodesorption of SO_4^{2-}

To confirm the applicability of the proposed technique to general anion electrodesorption, we matched the electrode configuration and predicted the complete desorption potential for the electrodesorption of SO_4^{2-} . Based on the electrochemical description of SO_4^{2-} , the complete desorption potential was calculated as -1.45 V, lower than that of Cl^- . Therefore, the graphite anode–titanium cathode electrode configuration was an appropriate choice for SO_4^{2-} electrodesorption. Figure 4a plots the experimentally obtained desorption efficiency of SO_4^{2-} at different desorption times. The electrodesorption results of SO_4^{2-} were improved from those of Cl^- ; and after 3 h, the desorption efficiency reached 100%, indicating that SO_4^{2-} desorption occurs more easily than Cl^- desorption because the complete desorption potential is lower than -1.7 V. The low cathode potential requirements were attributed to the weak chemical bonds between SO_4^{2-} and GAC [38,53]. In a previous report on the adsorption of sulfanilamide to activated carbon, the higher effect of Cl^- compared to SO_4^{2-} on the adsorption capacity was similarly attributed to different bond strengths (strong versus weak chemical bonds) [54]. Therefore, we speculate that the potential of complete desorption depends on the strength of the formative chemical bonds between the anions and electrode materials during the electrodesorption process.

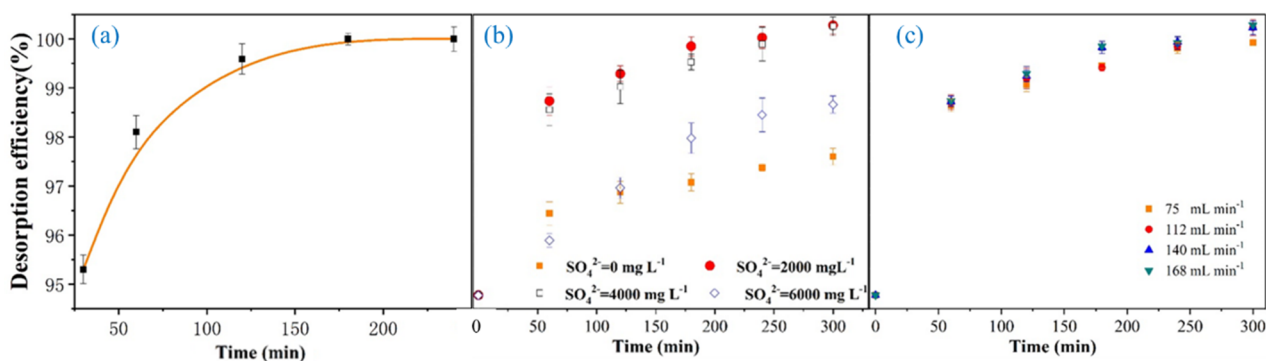


Figure 4. The desorption efficiency. (a) Study on the desorption efficiency of SO_4^{2-} . (b) Effect of the ionic strength on the Cl^- desorption efficiency. (c) Effect of circulation velocities on Cl^- desorption efficiency.

It is worth noting that the prediction of complete desorption potential is applicable only to anions with desorption ability under the same chemical conditions. Unlike Cl^- , anions such as ReO_4^- are not desorbed because they strongly adhere to GAC at the chemical condition of Cl^- desorption, as revealed in our previous work [38]. Therefore,

the application of a prediction method of desorption potential is not appropriate for the adsorption of ReO_4^- on GAC.

3.4. Effect of Ionic Strength

The effect of ionic strength was investigated by cycling desorptive solutions with $0.1 \text{ mol L}^{-1} \text{ Cl}^-$ and SO_4^{2-} ranging from 0 mg L^{-1} to 6000 mg L^{-1} . As shown in Figure 4b, the desorption efficiency first increases and then decreases with an increase in the ionic strength from 0 to 6000 mg L^{-1} . The highest desorption efficiency is obtained when the SO_4^{2-} concentrations are 2000 and 4000 mg L^{-1} , with values that are two times higher than that of $6000 \text{ mg L}^{-1} \text{ SO}_4^{2-}$, meaning that the desorption efficiency is strongly dependent on ionic strength. This phenomenon results from the fact that the EDL is compressed under a higher ionic strength [55,56], resulting in a lower diffuse layer potential (ψ). The electrode potential can be approximately represented by the diffuse layer potential; the desorption efficiency, therefore, decreases with an increase in ionic strength due to the lower cathode potential based on the electrodesorption mechanism. In addition, the decrease in the desorption efficiency in desorptive solutions without SO_4^{2-} is probably due to the lower solution conductivity.

3.5. Effect of Circulating Velocity

Ionic migration in CDI devices is dependent on the circulation of the solution. The effect of circulating velocity on the desorption process was studied at different circulating velocities of the solution, and the result is shown in Figure 4c. The desorption efficiencies after 5 h under circulating velocities of 75 , 112 , 140 , and 168 mL min^{-1} were approximately 94% , 100% , 100% , and 100% , respectively. It is worth noting that the higher circulating velocity caused a higher desorption efficiency. This trend seems to be in good agreement with other reports [19,57]. Circulating velocity increases convection, thereby reducing stagnant or boundary layer thickness that tends to accelerate ion transfer [58]. When the circulating velocity is 112 mL min^{-1} , the desorption efficiency reached the maximum of 100% , and the difference in desorption efficiency is not obvious when the circulation velocities are greater than 112 mL min^{-1} . This can be attributed to the electric field. Due to the electric field external to the electrode, mass transfer through the boundary layer will be enhanced [59,60]. Thus, the optimal circulating velocity is 112 mL min^{-1} .

4. Conclusions

We presented a graphite anode–titanium cathode electrode configuration that increases the cathode potential to -1.7 V . At an operating cathode potential of -1.7 V , the system provided an excellent (100%) electrodesorption performance and maintained this performance after five cycles. The boosting of the cathode potential was associated with the redox property of the electrode. Strengthening the oxidizability of the anode and the reducibility of the cathode, widened the cathode potential. Applying the optimal electrode configuration to SO_4^{2-} electrodesorption, the desorption efficiency remained at 100% after 3 h. The Cl^- desorption efficiency was found to depend on the ionic strength and was independent of circulating velocities exceeding 112 mL min^{-1} . Our approach can predict the cathode potential of complete desorption and can guide the design optimization of completely desorbing CDI devices.

Author Contributions: Investigation, writing—original draft preparation, data curation, formal analysis, J.F.; supervision, H.W.; supervision, R.J., supervision, Y.W.; conceptualization, P.L.; conceptualization, Y.L.; conceptualization, writing-review and editing, Q.W.; investigation, data curation, writing-review and editing, funding acquisition, Z.S. All authors have read and agreed to the published version of the manuscript.

Funding: This work was supported by the National Natural Science Foundation of China [52004256], the Shanxi Province Science Foundation for Youths [201901D211212], the Scientific and Technological Innovation Programs of Higher Education Institutions in Shanxi [2019L0574] and the Young academic leader of North University of China [QX202004].

Conflicts of Interest: The authors declare no competing financial interest.

References

1. Caudle, D.D.; Tucker, J.T.H.; Papastamataki, A. *Electrochemical Demineralization of Water with Carbon Electrodes*, Research Report; Oklahoma University Research Institute: Norman, OK, USA, 1966.
2. Anderson, M.A.; Cudero, A.L.; Palma, J. Capacitive deionization as an electrochemical means of saving energy and delivering clean water. Comparison to present desalination practices: Will it compete? *Electrochim. Acta* **2010**, *55*, 3845–3856. [[CrossRef](#)]
3. Gabelich, C.; Tran, T.; Suffet, I. Electrosorption of inorganic salts from aqueous solution using carbon aerogels. *Environ. Sci. Technol.* **2002**, *36*, 3010–3019. [[CrossRef](#)] [[PubMed](#)]
4. Gu, X.; Yang, Y.; Hu, Y.; Hu, M.; Wang, C. Fabrication of Graphene-Based Xerogels for removal of heavy metal ions and Capacitive Deionization. *ACS Sustain. Chem. Eng.* **2015**, *3*, 1056–1065. [[CrossRef](#)]
5. Han, L.; Karthikeyan, K.G.; Anderson, M.A.; Gregory, K.B. Exploring the impact of pore size distribution on the performance of carbon electrodes for capacitive deionization. *J. Colloid Interface Sci.* **2014**, *430*, 93–99. [[CrossRef](#)]
6. Zhang, Y.; Chen, L.; Mao, S.; Sun, Z.; Song, Y.; Zhao, R. Fabrication of porous graphene electrodes via CO₂ activation for the enhancement of capacitive deionization. *J. Colloid Interface Sci.* **2019**, *536*, 252–260. [[CrossRef](#)]
7. Porada, S.; Zhao, R.; Wal, A.; Presser, V.; Biesheuvel, P.M. Review on the science and technology of water desalination by capacitive deionization. *Prog. Mater. Sci.* **2013**, *58*, 1388–1442. [[CrossRef](#)]
8. Lee, J.; Jo, K.; Lee, J.; Hong, S.P.; Kim, S.; Yoon, J. Rocking-Chair capacitive deionization for continuous brackish water desalination. *ACS Sustain. Chem. Eng.* **2018**, *6*, 10815–10822. [[CrossRef](#)]
9. Xu, P.; Drewes, J.E.; Heil, D.; Wang, G. Treatment of brackish produced water using carbon aerogel-based capacitive deionization technology. *Water Res.* **2008**, *42*, 2605–2617. [[CrossRef](#)]
10. Lado, J.J.; Zornitta, R.L.; Calvi, F.A.; Tejedor-Tejedor, M.I.; Anderson, M.A.; Ruotolo, L.A.M. Study of sugar cane bagasse fly ash as electrode material for capacitive deionization. *J. Anal. Appl. Pyrol.* **2016**, *120*, 389–398. [[CrossRef](#)]
11. Suss, M.E.; Porada, S.; Sun, X.; Biesheuvel, P.M.; Yoon, J.; Presser, V. Water desalination via capacitive deionization: What is it and what can we expect from it? *Energ. Environ. Sci.* **2015**, *8*, 2296–2319. [[CrossRef](#)]
12. Chong, L.G.; Chen, P.A.; Huang, J.Y.; Huang, H.L.; Wang, H.P. Capacitive deionization of a RO brackish water by AC/graphene composite electrodes. *Chemosphere* **2018**, *191*, 296–301. [[CrossRef](#)] [[PubMed](#)]
13. Oren, Y. Capacitive deionization (CDI) for desalination and water treatment—Past, present and future (a review). *Desalination* **2008**, *228*, 10–29. [[CrossRef](#)]
14. Ban, A.; Schafer, A.; Wendt, H. Fundamentals of electrosorption on activated carbon for wastewater treatment of industrial effluents. *J. Appl. Electrochem.* **1998**, *28*, 227–236. [[CrossRef](#)]
15. Oh, H.-J.; Lee, J.-H.; Ahn, H.-J.; Jeong, Y.; Kim, Y.-J.; Chi, C.-S. Nanoporous activated carbon cloth for capacitive deionization of aqueous solution. *Thin Solid Films* **2006**, *515*, 220–225. [[CrossRef](#)]
16. Kim, S.; Yoon, J.; Yoon, H.; Shin, D.; Lee, J. Electrochemical selective ion separation in capacitive deionization with sodium manganese oxide. *J. Colloid Interface Sci.* **2017**, *506*, 644–648. [[CrossRef](#)]
17. Chao, L.; Liu, Z.; Zhang, G.; Song, X.; Lei, X.; Noyong, M.; Simon, U.; Chang, Z.; Sun, X. Enhancement of capacitive deionization capacity of hierarchical porous carbon. *J. Mater. Chem. A* **2015**, *3*, 12730–12737. [[CrossRef](#)]
18. Lee, J.; Bae, W.; Choi, J. Electrode reactions and adsorption/desorption performance related to the applied potential in a capacitive deionization process. *Desalination* **2010**, *258*, 159–163. [[CrossRef](#)]
19. Lado, J.J.; Pérez-Roa, R.E.; Wouters, J.J.; Tejedor-Tejedor, M.I.; Anderson, M.A. Evaluation of operational parameters for a capacitive deionization reactor employing asymmetric electrodes. *Sep. Purif. Technol.* **2014**, *133*, 236–245. [[CrossRef](#)]
20. Bayram, E.; Hoda, N.; Ayranci, E. Adsorption/electrosorption of catechol and resorcinol onto high area activated carbon cloth. *J. Hazard. Mater.* **2009**, *168*, 1459–1466. [[CrossRef](#)]
21. Lado, J.J.; Pérez-Roa, R.E.; Wouters, J.J.; Tejedor-Tejedor, M.I.; Federspill, C.; Ortiz, J.M.; Anderson, M.A. Removal of nitrate by asymmetric capacitive deionization. *Sep. Purif. Technol.* **2017**, *183*, 145–152. [[CrossRef](#)]
22. Villar, I.; Roldan, S.; Ruiz, V.; Granda, M.; Blanco, C.; Menéndez, R.; Santamaría, R. Capacitive deionization of NaCl solutions with modified activated carbon electrodes. *Energy Fuel* **2010**, *24*, 3329–3333. [[CrossRef](#)]
23. Wu, Z.Y.; Liu, Y.; Wang, S.Y.; Peng, P.; Li, X.Y.; Xu, J.; Li, W.H. A novel integrated system of three-dimensional electrochemical reactors (3DERs) and three-dimensional biofilm electrode reactors (3DBERs) for coking wastewater treatment. *Bioresour. Technol.* **2019**, *284*, 222–230. [[CrossRef](#)] [[PubMed](#)]
24. Xue, Y.; Feng, C. Achieving high performance for electrocatalytic dechlorination with magnetic Pd/CoFe₂O₄ particle electrodes. *Appl. Surf. Sci.* **2021**, *545*, 149007. [[CrossRef](#)]
25. Pang, T.; Wang, Y.; Yang, H.; Wang, T.; Cai, W. Dynamic model of organic pollutant degradation in three dimensional packed bed electrode reactor. *Chemosphere* **2018**, *206*, 107–114. [[CrossRef](#)]

26. Chen, H.; Feng, Y.; Suo, N.; Long, Y.; Li, X.; Shi, Y.; Yu, Y. Preparation of particle electrodes from manganese slag and its degradation performance for salicylic acid in the three-dimensional electrode reactor (TDE). *Chemosphere* **2019**, *216*, 281–288. [[CrossRef](#)]
27. Cho, S.; Kim, C.; Hwang, I. Electrochemical degradation of ibuprofen using an activated-carbon-based continuous-flow three-dimensional electrode reactor (3DER). *Chemosphere* **2020**, *259*, 127382. [[CrossRef](#)]
28. Xu, L.N.; Zhao, H.Z.; Ni, J.R. Effect of cathode material on electrolytic treatment of Acid Orange 7 by a three-phase three-dimensional electrode reactor. *Huan Jing Ke Xue* **2008**, *29*, 942–947.
29. Lv, G.; Chen, Y.; Yang, T.; Li, J. Electrocatalytic Oxidation Removal of Phenol from Aqueous Solution with Metal Oxides Doped Carbon Aerogel. *J. Braz. Chem. Soc.* **2017**, *29*, 689–694. [[CrossRef](#)]
30. Oda, H.; Nakagawa, Y. Removal of ionic substances from dilute solution using activated carbon electrodes. *Carbon* **2003**, *41*, 1037–1047. [[CrossRef](#)]
31. Gaikwad, M.S.; Balomajumder, C. Tea waste biomass activated carbon electrode for simultaneous removal of Cr(VI) and fluoride by capacitive deionization. *Chemosphere* **2017**, *184*, 1141–1149. [[CrossRef](#)]
32. Ye, W.; Zhang, W.; Hu, X.; Yang, S.; Liang, W. Efficient electrochemical-catalytic reduction of nitrate using Co/AC0.9-AB0.1 particle electrode. *Sci. Total Environ.* **2020**, *732*, 139245. [[CrossRef](#)] [[PubMed](#)]
33. Huang, S.; Lu, Y.; Li, X.; Lu, Y.; Zhu, G.; Hassan, M. Tertiary denitrification and organic matter variations of secondary effluent from wastewater treatment plant by the 3D-BER system. *Environ. Res.* **2020**, *189*, 109937. [[CrossRef](#)] [[PubMed](#)]
34. Li, J.; Gao, F. Analysis of electrodes matching for asymmetric electrochemical capacitor. *J. Power Sources* **2009**, *194*, 1184–1193. [[CrossRef](#)]
35. Laxman, K.; Gharibi, L.A.; Dutta, J. Capacitive deionization with asymmetric electrodes: Electrode capacitance vs electrode surface area. *Electrochim. Acta* **2015**, *176*, 420–425. [[CrossRef](#)]
36. Sun, Z.; Chai, L.; Shu, Y.; Li, Q.; Liu, M. Chemical bond between chloride ions and surface carboxyl groups on activated carbon. *Colloid Surf. A Physicochem. Eng. Asp.* **2017**, *530*, 53–59. [[CrossRef](#)]
37. Sun, Z.; Chai, L.; Liu, M.; Shu, Y.; Li, Q. Capacitive deionization of chloride ions by activated carbon using a three-dimensional electrode reactor. *Sep. Purif. Technol.* **2018**, *191*, 424–432. [[CrossRef](#)]
38. Sun, Z.; Chai, L.; Liu, M.; Shu, Y.; Li, Q.; Wang, Y.; Qiu, D. Effect of the electronegativity on the electrosorption selectivity of anions during capacitive deionization. *Chemosphere* **2018**, *195*, 282–290. [[CrossRef](#)]
39. Park, K.H.; Kwak, D.H. Electrosorption and electrochemical properties of activated-carbon sheet electrode for capacitive deionization. *J. Electroanal. Chem.* **2014**, *732*, 66–73. [[CrossRef](#)]
40. Zhang, G.; He, Z.; Xu, W. A low-cost and high efficient zirconium-modified-Na-attapulgite adsorbent for fluoride removal from aqueous solutions. *Chem. Eng. J.* **2012**, *183*, 315–324. [[CrossRef](#)]
41. Lai, Y.; Liu, W.; Chen, L.; Chang, M.; Lee, C.; Tai, N. Electro-assisted selective uptake/release of phosphate using a graphene oxide/MgMn-layered double hydroxide composite. *J. Mater. Chem. A* **2019**, *7*, 3962–3970. [[CrossRef](#)]
42. Yang, K.; Ying, T.; Yiacoymi, S.; Tsouris, A.C.; Vittoratos, E. Electrosorption of ions from aqueous solutions by carbon aerogel: An electrical double layer model. *Langmuir* **2001**, *17*, 1961–1969. [[CrossRef](#)]
43. Sun, Z.; Li, Q.; Chai, L.; Shu, Y.; Wang, Y.; Qiu, D. Effect of the chemical bond on the electrosorption and desorption of anions during capacitive deionization. *Chemosphere* **2019**, *229*, 341–348. [[CrossRef](#)] [[PubMed](#)]
44. Biesheuvel, P.M.; van Limpt, B.; van der Wal, A. Dynamic adsorption/desorption process model for capacitive deionization. *J. Phys. Chem. C* **2009**, *113*, 5636–5640. [[CrossRef](#)]
45. Xing, W.; Liang, J.; Tang, W.; Zeng, G.; Wang, X.; Li, X.; Jiang, L.; Luo, Y.; Li, X.; Tang, N.; et al. Perchlorate removal from brackish water by capacitive deionization: Experimental and theoretical investigations. *Chem. Eng. J.* **2019**, *361*, 209–218. [[CrossRef](#)]
46. He, D.; Chi, E.W.; Tang, W.; Kovalsky, P.; Waite, T.D. Faradaic reactions in water desalination by batch-mode Capacitive Deionization. *Environ. Sci. Technol. Lett.* **2016**, *3*, 222–226. [[CrossRef](#)]
47. Comninellis, C.; Nerini, A. Anodic oxidation of phenol in the presence of NaCl for wastewater treatment. *J. Appl. Electrochem.* **1995**, *25*, 23–28. [[CrossRef](#)]
48. Martínez-Huitle, C.A.; Rodrigo, M.A.; Sirés, I.; Scialdone, O. Single and coupled electrochemical processes and reactors for the abatement of organic water pollutants: A critical review. *Chem. Rev.* **2015**, *115*, 13362–13407. [[CrossRef](#)]
49. Jung, Y.J.; Baek, K.W.; Oh, B.S.; Kang, J.-W. An investigation of the formation of chlorate and perchlorate during electrolysis using Pt/Ti electrodes: The effects of pH and reactive oxygen species and the results of kinetic studies. *Water Res.* **2010**, *44*, 5345–5355. [[CrossRef](#)]
50. Xiao, Y.; Hill, J.M. Mechanistic insights for the electro-Fenton regeneration of carbon materials saturated with methyl orange: Dominance of electrodesorption. *J. Hazard. Mater.* **2019**, *367*, 59–67. [[CrossRef](#)]
51. Lee, D.H.; Ryu, T.; Shin, J.; Ryu, J.C.; Chung, K.S.; Kim, Y.H. Selective lithium recovery from aqueous solution using a modified membrane capacitive deionization system. *Hydrometallurgy* **2017**, *173*, 283–288. [[CrossRef](#)]
52. None, Lead oxidation work may lead to standards. *Chem. Eng. News* **1966**, *44*, 51.
53. Xiong, W.; Tong, J.; Yang, Z.; Zeng, G.; Zhou, Y.; Wang, D.; Song, P.; Xu, R.; Zhang, C.; Cheng, M. Adsorption of phosphate from aqueous solution using iron-zirconium modified activated carbon nanofiber: Performance and mechanism. *J. Colloid Interface Sci.* **2017**, *493*, 17–23. [[CrossRef](#)] [[PubMed](#)]

54. Xu, T.; Du, J.; Zhang, J.; David, W.; Liu, P.; Faheem, M.; Zhu, X.; Yang, J.; Bao, J. Microbially-mediated synthesis of activated carbon derived from cottonseed husks for enhanced sulfanilamide removal. *J. Hazard. Mater.* **2022**, *426*, 127811. [[CrossRef](#)]
55. Yang, K.L.; Yiacoumi, S.; Tsouris, C. Proton adsorption and electrical double-layer formation inside charged platinum nanochannels. *Nano Lett.* **2004**, *2*, 1433–1437. [[CrossRef](#)]
56. Ying, T.Y.; Yang, K.L.; Yiacoumi, S.; Tsouris, C. Electrosorption of ions from aqueous solutions by nanostructured carbon aerogel. *J. Colloid Interface Sci.* **2002**, *250*, 18–27. [[CrossRef](#)]
57. Bo, S.; Luo, J.; An, Q.; Xiao, Z.; Wang, H.; Cai, W.; Zhai, S.; Li, Z. Efficiently selective adsorption of Pb(II) with functionalized alginate-based adsorbent in batch/column systems: Mechanism and application simulation. *J. Clean. Prod.* **2020**, *250*, 119585. [[CrossRef](#)]
58. Han, L.; Karthikeyan, K.G.; Anderson, M.A.; Wouters, J.J.; Gregory, K.B. Mechanistic insights into the use of oxide nanoparticles coated asymmetric electrodes for capacitive deionization. *Electrochim. Acta* **2013**, *90*, 573–581. [[CrossRef](#)]
59. Godino, M.P.; Barragán, V.M.; Izquierdo, M.A.; Villaluenga, J.P.G.; Seoane, B.; Ruiz-Bauzá, C. Study of the activation energy for transport of water and methanol through a Nafion membrane. *Chem. Eng. J.* **2009**, *152*, 20–25. [[CrossRef](#)]
60. Qu, Y.; Campbell, P.G.; Hemmatifar, A.; Knipe, J.M.; Loeb, C.K.; Reidy, J.J.; Hubert, M.A.; Stadermann, M.; Santiago, G.J. Charging and Transport Dynamics of a Flow-Through Electrode Capacitive Deionization System. *J Phys. Chem. B* **2018**, *122*, 240–249. [[CrossRef](#)]